Nanographene-Constructed Carbon Nanofibers Grown on Graphene Sheets by Chemical Vapor Deposition: High-Performance Anode Materials for Lithium Ion Batteries

Zhuang-Jun Fan,[†,*] Jun Yan,[†] Tong Wei,[†] Guo-Qing Ning,[‡] Lin-Jie Zhi,[§,*] Jin-Cheng Liu,[†] Dian-Xue Cao,[†] Gui-Ling Wang,[†] and Fei Wei[⊥,*]

[†]Key Laboratory of Superlight Materials and Surface Technology, Ministry of Education, College of Material Science and Chemical Engineering, Harbin Engineering University, Harbin 150001, China, [‡]State Key Laboratory of Heavy Oil Processing, China University of Petroleum, Beijing 102249, China, [§]National Center for Nanoscience and Technology of China, Zhongguancun, Beiyitiao 11, Beijing 100190, China, and [⊥]Beijing Key Laboratory of Green Chemical Reaction Engineering and Technology, Department of Chemical Engineering, Tsinghua University, Beijing 100084, China.

ABSTRACT We report on the fabrication of 3D carbonaceous material composed of 1D carbon nanofibers (CNF) grown on 2D graphene sheets (GNS) *via* a CVD approach in a fluidized bed reactor. Nanographene-constructed carbon nanofibers contain many cavities, open tips, and graphene platelets with edges exposed, providing more extra space for Li^+ storage. More interestingly, nanochannels consisting of graphene platelets arrange almost perpendicularly to the fiber axis, which is favorable for lithium ion diffusion from different orientations. In addition, 3D interconnected architectures facilitate the collection and transport of electrons during the cycling process. As a result, the CNF/GNS hybrid material shows high reversible capacity (667 mAh/g), high-rate performance, and cycling stability, which is superior to those of pure graphene, natural graphite, and carbon nanotubes. The simple CVD approach offers a new pathway for large-scale production of novel hybrid carbon materials for energy storage.

KEYWORDS: graphene nanosheets · carbon nanofibers · lithium ion battery

The storage of electrical energy at high charge and discharge rate is an important technology in today's society and can enable portable electronic devices and plug-in hybrid electric vehicles.[1,2] Recently, the design and fabrication of three-dimensional (3D) multifunctional architectures from the appropriate nanoscale building blocks, including the strategic use of void space, have attracted great attention in energy storage application.[3] For 3D carbon architectures, the prime advantages are the short transport lengths for ions in the solid-state electrode and well-interconnected wall structure, providing a continuous electron pathway, yielding fast transport channels, as ions in electrolytes can be easily accessible to the 3D pore surfaces.

Graphene, a two-dimensional nanostructure of carbon, is recently expected to be an advanced energy storage material due to its high surface area to volume ratio, extraordinary electronic transport properties, and chemical stability.[4−22] Results have shown that, by controlling the composition and architecture at the nano/micrometer scale, graphene hybrid material with carbon nanotubes (CNTs) may prove to be especially useful for application in electronic devices and energy storage materials.[23] Currently, the trends are to integrate them into a hybrid material through three versatile fabrication techniques: electrostatic self-assembly;[23−25] a simple mixing method with the assistance of ultrasonic treatment;[4,26,27] and chemical vapor deposition (CVD).[28−30] For example, the introduction of CNTs into graphene films considerably decreased the sheet resistance of the films.[23] Hybrid films of graphene and CNTs, sequentially self-assembled *via* electrostatic interactions, exhibited a nearly rectangular cyclic voltammogram even at a high scan rate of 1 V/s with an average specific capacitance of 120 F/g.[24] Altogether graphene incorporation of CNTs *via* a simple mixing process exhibited a large enhancement of capacity from the expansion of the interlayer spacing.[4] Because graphene sheets have low conductivity in the vertical direction and easily form irreversible agglomerates through van der Waals interactions, to improve high-rate performance for energy storage, it is important to make full use of the graphene layer as more favorable

* Address correspondence to fanzhj666@163.com; zhilj@nanoctr.cn; weifei@flotu.org.

Received for review November 28, 2010 and accepted March 22, 2011.

Published online March 22, 2011
10.1021/nn200195k

sites for additional energy storage and construct the overall conductivity of graphene networks.[16,31,32] Here, we report on the fabrication of 3D carbon nanofiber/graphene consisting of 1D carbon nanofibers (CNF) on 2D graphene sheets (GNS) *via* a CVD approach in a fluidized bed reactor, as demonstrated in Scheme 1. Thereby, we employ graphene oxide as catalyst support to deposit nanofibers on the graphene sheet stemming from the pyrolysis of graphene oxide during the CVD process. These carbon nanofibers have many cavities, open tips, and graphene platelets having more edges exposed, providing more extra space for Li^+ storage. More interestingly, nanochannels consisting of graphene platelets arrange almost perpendicularly to the fiber axis, which is favorable for lithium ion diffusion from different orientations; 3D interconnected architectures facilitate the collection and transport of electrons during the cycling process. Preliminary studies of the GNS/CNF as anode material for a Li ion battery show high reversible capacity (~667 mAh/g), high-rate performance, and cycling stability.

RESULTS AND DISCUSSION

Most of the carbon nanofibers grown on graphite substrate are not uniform due to the poor wettability between the graphite surface and the metallic catalyst particles, which results in aggregation and then coalescence of the catalyst on the graphite substrate during sintering.[33] Therefore, exfoliated graphene oxide (GO, ~1 nm in thickness, Figure 1A,B) is selected here as a catalyst support to grow nanofibers due to its high surface energy (62.1 mJ/m^2) and oxygen content (C/O atomic ratio of 2).[34] As a result, cobalt precursor particles with a size of 2−5 nm uniformly deposit on the surface of GO after microwave irradition (Figure 1C). Energy dispersive X-ray spectra (EDX) shows that the weight percent of cobalt is 8%. For the CNF/GNS composite, CNFs with a length less than 1 μm are distributed in between the graphene sheets (Figure 1D, E). Indeed, the BET surface area of CNF/GNS (315 m^2/g) is higher than that of graphene (202 m^2/g) due to the effective CNF intercalation into graphene. Under fluidization conditions, super-lightweight catalyst supports are randomly oriented in the whole fluidized bed during the CVD process; the gradients of temperature and carbon source concentration cause a discontinuous carbon growth. Therefore, the formation of a segmented structure is due to the unsaturation of carbon concentration on the deposition faces.[35] TEM observations exhibit that the obtained nanofiber with an outer diameter of about 20 nm (Figure 1F) consists of well-ordered graphene platelets (Figure 1G) with a spacing of 0.342 nm, which is close to the ideal graphite lattice.[36] Moreover, the path of the cobalt catalyst from the axis to the edge of the fiber is

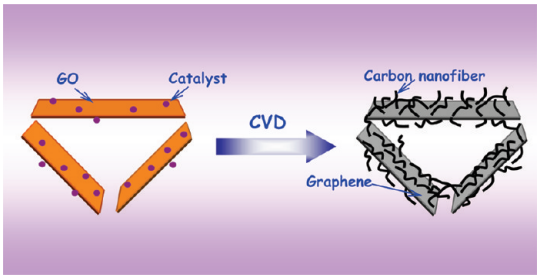

Scheme 1. Illustrations of the fabrication of GNS/CNF composite *via* a CVD approach using a fluidized bed reactor.

observed due to the blowing gas (Figure 1H). The formation of many hollow cavities along the fiber axis (Figure 1F) can provide extra space for Li storage, confirming a discontinuous growth. Notably, the HRTEM image (Figure 2A) of the nanofiber shows that the nanochannels composed of edge-exposed graphene platelets arrange almost perpendicularly to the fiber axis, which is favorable for lithium ion diffusion from different orientations and sufficient contact between active materials and electrolyte.[37]

Also, open-ended CNFs are clearly observed in Figure 2B−D (marked by arrows), which is beneficial to the reduction of the effective diffusion distance for Li ions. This phenomenon can be explained by the liquid metal catalyst running off due to the blowing gas during the CVD process (Figure 1H), resulting in subsequent growth of a thin fiber (Figure 2C). Because of the random gas flow direction, a twisted fiber is also observed in Figure 2D.

The cobalt catalyst is observed on the CNF tip (Figure 1F), confirming a tip growth model due to the poor binding strength between the catalyst and graphene.[33] The catalyst on the CNF tip means that the Co particle remains active and exposed to carbon from the vapor phase during the growth. As confirmed by XRD analysis (Figure 3A), cobalt metal exists in the CNF/GNS composite. Moreover, the C(002) diffraction peak of the CNF/GNS composite, including graphene sheets and nanofibers, is sharp, meaning a well-graphitized structure. Notably, graphene sheets of GNS/CNF are found to possess a higher average *d*-spacing of approximately 0.414 nm compared to those of GNS (0.363 nm) and CNTs (0.344 nm), implying that CNF grows in between the graphene layers.[4]

Raman scattering is strongly sensitive to the electronic structure and proves to be an essential tool to characterize graphite and graphene materials. In many cases, the Raman spectrum of graphene is characterized by two main features, the G mode, arising from the first-order scattering of the E_{2g} phonon of sp^2 C atoms (usually observed at ~1575 cm^{-1}), and the D mode, arising from a breathing mode of κ-point photons of A_{1g} symmetry (~1350 cm^{-1}).[38,39] In our study, Raman characterization (Figure 3B) demonstrates that the

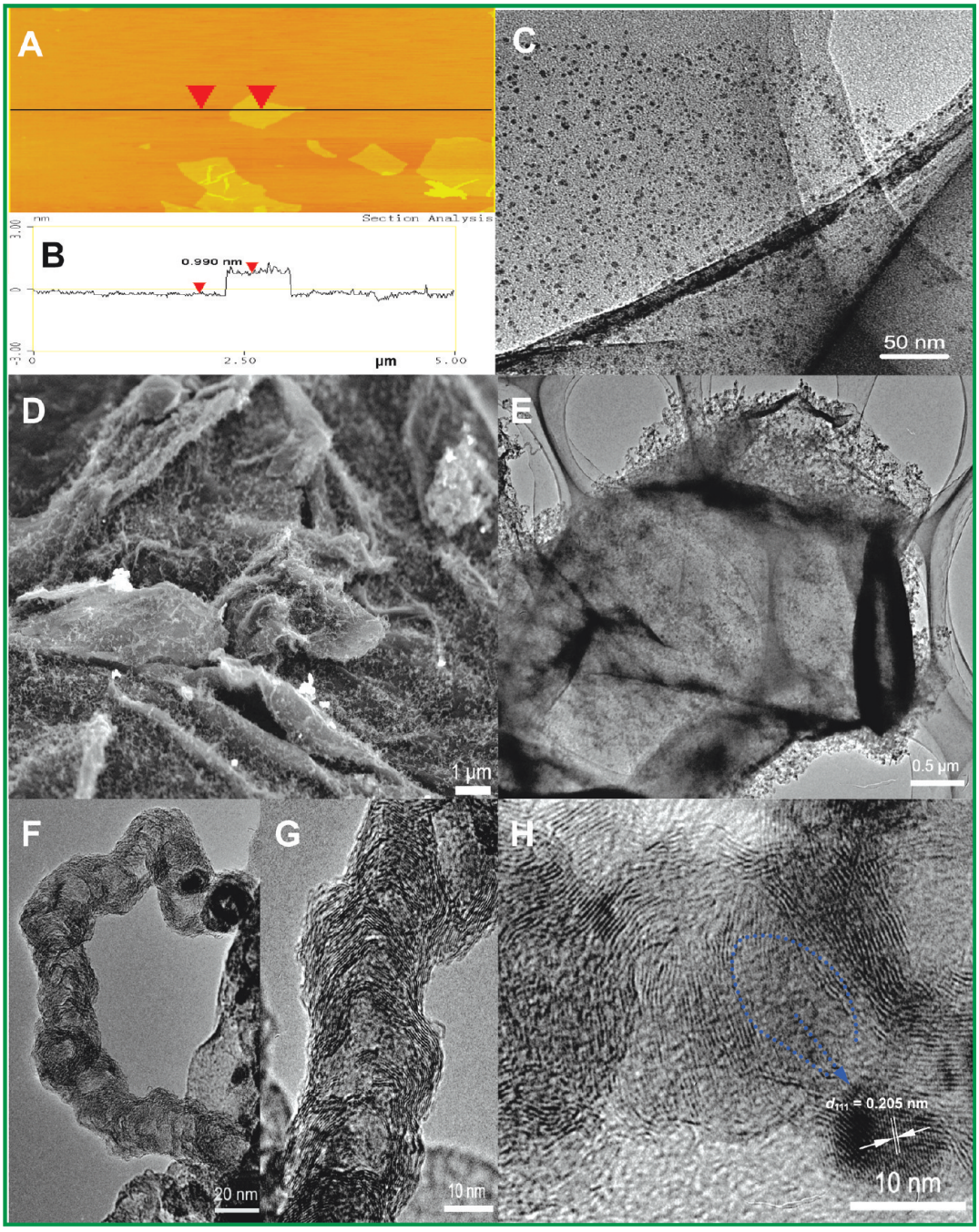

Figure 1. (A) AFM image of GO dispersed on mica and (B) corresponding line profile.(C) TEM image of cobalt catalyst on GO. (D) SEM image of CNF/GNS composite. (E, F) Low-magnification TEM. (G, H) HRTEM images of CNF/GNS composite. The blue dotted circle in (H) indicates the original catalyst site.

intensity ratio (I_D/I_G) of D and G bands of GNS is about 1.02, whereas the I_D/I_G of GNS/CNF is 1.06, implying a graphitic crystalline structure.[40]

The electrochemical performance of the as-prepared GNS/CNF composite was first evaluated by galvanostatic charge/discharge cycling at the current density of 0.12 mA/cm^2. For comparison, we also present the result of pure graphene under the same electrochemical conditions. In the first cycle (Figure 4A), GNS/CNF delivers a very high reversible capacity (667 mAh/g) in the voltage range of 0.05 to 3.0 V (vs Li^+/Li), which is 80% higher than that of graphite (theoretical specific capacity of 372 mAh/g) and is also higher than that of pure graphene (453 mAh/g). The capacity of GNS/CNF is comparable with other nanostructured carbon electrode materials, such as hollow carbon spheres (600 mAh/g)[41] and CNF/CNT(546 mAh/g).[42] Owing to high content of CNF on GNS, the capacity of GNS/CNF is slightly less than that of GNS/CNT (730 mAh/g).[4] Figure 4B shows the cyclic voltammograms of the GNS/CNF electrode at 0.1 mV/s. There is obvious cathodic current peak at approximately 1.20 V in the

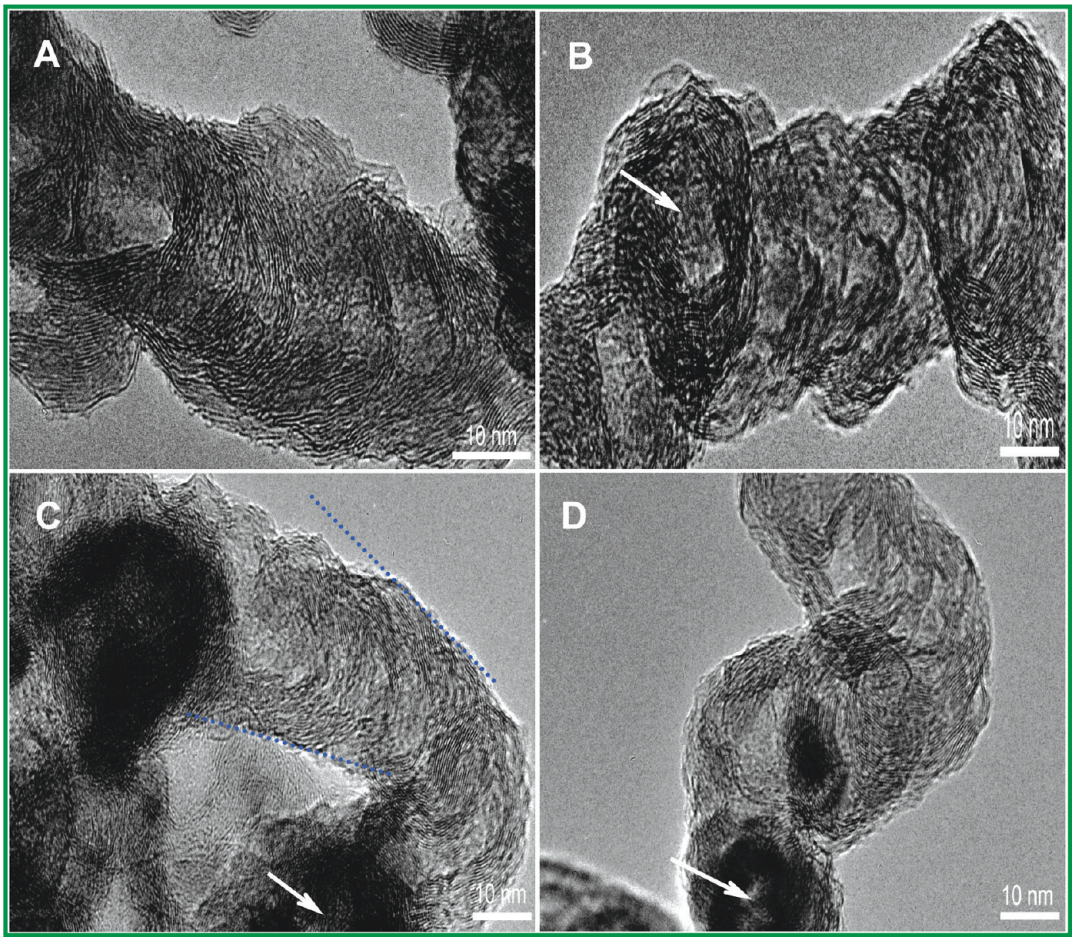

Figure 2. HRTEM images of nanofibers on a graphene sheet. Nanofibers showing well-ordered graphene platelets arranged almost perpendicularly to the fiber axis (A), open tips marked by arrows (B, C, D), and twisted growth (D). The blue dotted lines in (C) indicate that the diameter of nanofiber becomes smaller.

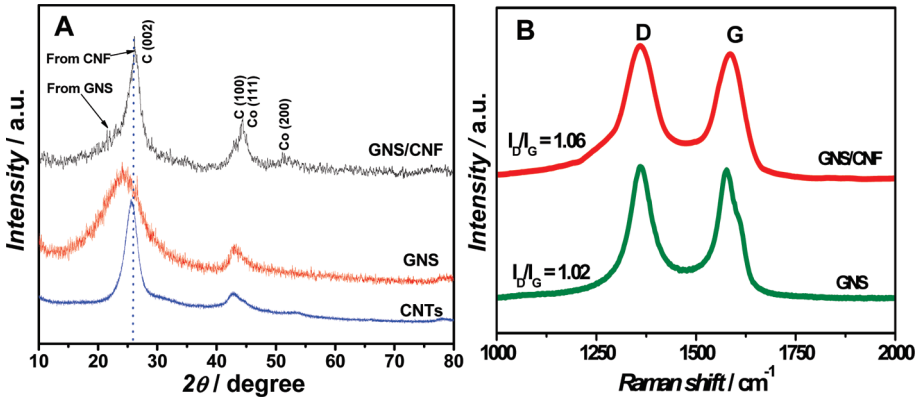

Figure 3. (A) XRD patterns of GNS/CNF, pure GNS, and CNTs. (B) Raman spectra of GNS/CNF and pure GNS. The blue dotted line in (A) indicates the (002) diffraction peak of graphite.

first cycle, which corresponds to the irreversible reactions between Li ions and electrolytes.[43]

Moreover, GNS/CNF exhibits a moderate Coulombic efficiency of about 55% in the first cycle due to the electrolyte decomposition and formation of the solid electrolyte interface (SEI) layer on the surface of the carbon (Figure 4A). Furthermore, the shape of the discharge and charge curves is similar to those observed previously from carbon nanotube materials.[44] Therefore, the Li storage in the GNS/CNF electrode is divided into two stages; the capacity of the potential region lower than 0.5 V (*vs* Li/Li^+, Figure 4A) should be due to lithium intercalation into the graphene layers, and the capacity above 0.5 V *vs* Li/Li^+ may be associated with Li storage onto the graphene surface or on the edge plane.[44] However, after the

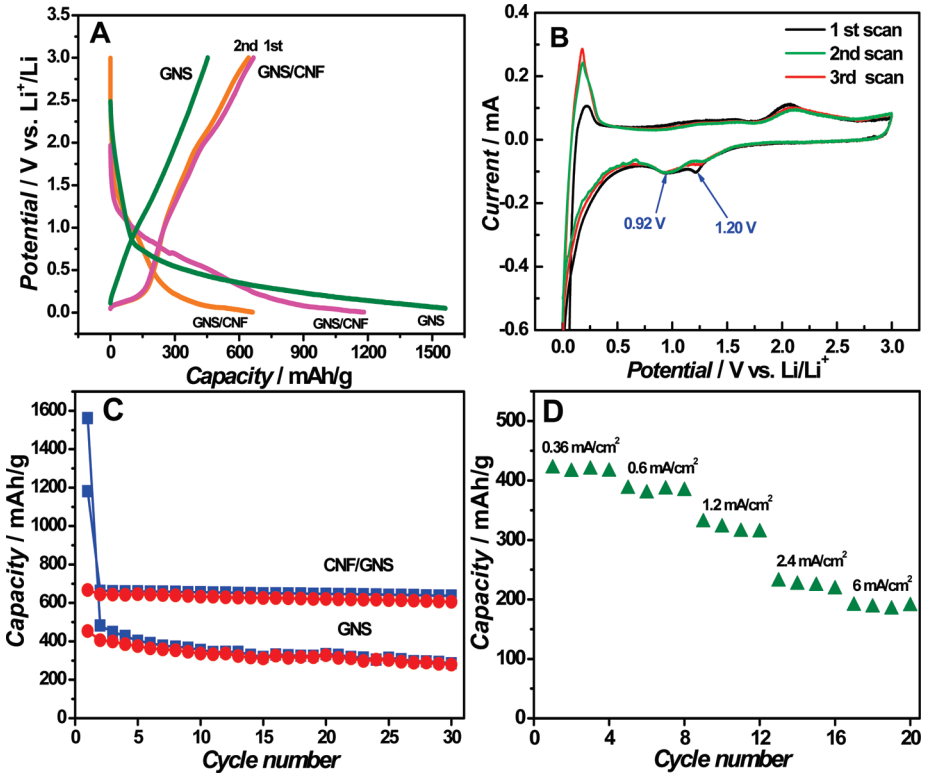

Figure 4. (A) Galvanostatic charge/discharge curves of GNS and GNS/CNF electrodes at a current density of 0.12 mA/cm^2. (B) Cyclic voltammograms of GNS/CNF in $LiPF_6$ with Li as counter and reference electrode at a scan rate of 0.1 mV/s. (C) Cycling performances of GNS and GNS/CNF electrodes at a current density of 0.12 mA/cm^2. (D) Rate performances of the CNF/GNS electrode at different current densities.

initial cycle (Figure 4C), the electrode becomes highly reversible (>98%). More importantly, the CNF/GNS composite exhibits a much better cycling performance than pure graphene (Figure 4C). It can be seen that the reversible capacity of CNF/GNS after 30 cycles at 0.12 mA/cm^2 decreases by 9%, and for pure graphene by 38%, respectively. On the basis of the above results, there is a strong synergistic effect between nanofibers and graphene sheets in the composite, which becomes much more apparent with higher cycle number and plays a central role in the excellent cyclic performance of the CNF/GNS composite.

Rate capability is an important factor for the use of lithium ion batteries (LIBs) in power applications. A good electrochemical energy storage device is required to provide its high energy density (specific capacitance) at a high charge/discharge rate.[31,32] The rate performance of the GNS/CNF electrode is shown in Figure 4D. At current densities of 0.36, 0.6, 1.2, 2.4, and 6 mA/cm^2, the reversible capacities of GNS/CNF reach *ca.* 420, 385, 329, 229, and 189 mAh/g, respectively, which are higher than those of GNS, CNT, CNF, CNF/natural graphite, and natural graphite (Figure 5). The results imply that the 3D carbon nanostructure of GNS/CNF is robust and very effective for improving the rate performance.

To understand the reasons for the excellent rate capability of GNS/CNF, electrochemical impedance

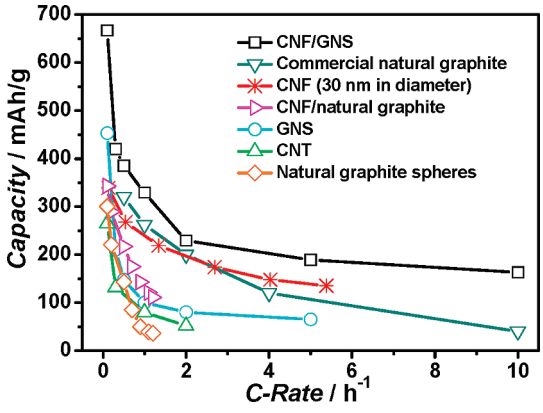

Figure 5. Comparison of the rate capabilities of CNF/GNS, GNS, CNT, commercial natural graphite discharged at C/5,[45] CNF (30 nm in diameter),[46] CNF/natural graphite,[47] and natural graphite spheres.[47]

spectroscopy (EIS) measurements were carried out after the 20th cycle at a rate of 0.5C (Figure 6). In general, the high-frequency semicircle (R_f) corresponds to the formation of an SEI film and/or contact resistance, and the charge-transfer resistance R_{ct} is assigned to the charge-transfer impedance on the electrode/electrolyte interface; the inclined line at an approximate 45° angle to the real axis corresponds to the lithium-diffusion process within the carbon electrodes.[48,49] Apparently, the values of R_f and R_{ct} for the GNS/CNF electrode decrease by a

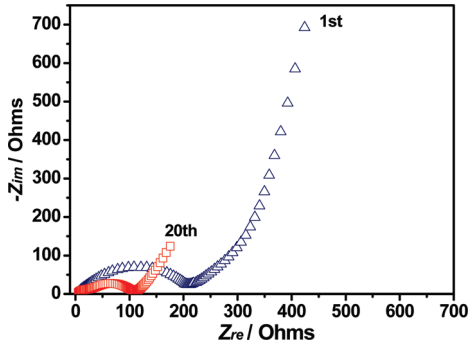

Figure 6. Nyquist plots of the GNS/CNF electrode after the first and 20th cycle with an amplitude of 5.0 mV in the frequency range from 100 kHz to 10 mHz.

factor of 2 after 20 cycles, implying that the GNS/CNF electrode possess a high electrical conductivity and a rapid charge-transfer reaction for lithium ion insertion and extraction. This can be further supported by simulating their kinetic parameters *via* the typical Randles equivalent circuit.[49] As expected, the exchange-current density i_o of GNS/CNF is increased by a factor of 2 after the 20th cycle, implying that the electrochemical activity of GNS/CNF is enhanced.

As a combination of the highly reversible capacity, excellent cyclic performance, and high-rate performance, the GNS/CNF electrode is a promising candidate anode material for high-performance LIBs. Though the high surface area of the GNS/CNF composite leads to a large irreversible capacity loss due to the electrolyte decomposition and formation of an SEI layer in the first cycle, the porous structure of GNS/CNF can supply a reduced effective diffusion distance for Li ions and buffer against the local volume change during Li insertion/desertion, resulting in better rate capability and cycling performance.[31,50] In addition, such pronounced electrochemical performance can be ascribed to the unique structure of CNF/GNS with a variety of favorable properties, as shown in Figure 7. First, the 3D carbon network acts as a structural buffer

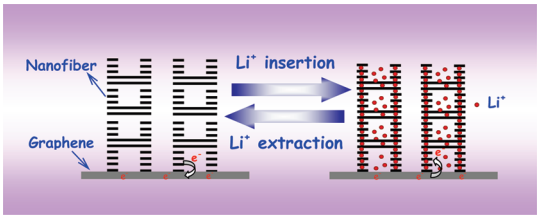

Figure 7. Discharge (Li^+ insertion) and charge (Li^+ extraction) processes of the GNS/CNF electrode.

for the large expansion/shrinkage of volume during the Li insertion/extraction, enabling good electrical contact during the cycling process.[51] Second, many cavities, open tips, and edge-exposed graphene platelets for the nanofibers can provide extra space, and the micro-nanochannel among graphene platelets and nanofibers is beneficial for the fast ion transfer and reduced diffusion paths for Li^+ storage. Finally, the 3D interconnected architecture maintains mechanical integrity and high electrical conductivity of the overall electrode.

CONCLUSIONS

We developed a simple process for the fabrication of 3D CNF/GNS hybrid material *via* a CVD approach. The nanofibers with many cavities, open tips, and edges of exposed graphene platelets are homogeneously distributed in between the graphene sheets as spacers to separate the neighboring graphene and are beneficial for fast ion/electron transfer and sufficient contact between active materials and electrolyte. Moreover, the synergistic effect between nanofibers and graphene sheets is beneficial for efficiently preventing volume expansion/shrinkage, resulting in good electrical contact during the cycling process. As a result, this hybrid material shows a significant fully reversible capacity (667 mAh/g), high-rate performance, and cycling stability. The simple CVD approach offers a new pathway for large-scale production of novel hybrid carbon materials for energy storage.

EXPERIMENTAL SECTION

Material Synthesis. Graphite oxide was synthesized from natural graphite (300 μm, Qingdao Graphite Company) by a modified Hummers method.[52] As-synthesized GO was suspended in water to give a brown suspension, which was subjected to dialysis to completely remove residual salts and acids. Exfoliation of 0.2 g of GO was achieved by ultrasonication in an ultrasonic bath (KQ-600KDE, 600 W). After that, 0.2 g of $Co(NO_3)_2 \cdot 6H_2O$ and 0.8 g of urea were added into the above suspension. Subsequently, the resulting suspension was heated using a microwave oven (Haier, 2450 MHz, 700 W) for 15 min. After filtration and desiccation, the sample was placed in a fluidized bed reactor and heated to 700 at 20 °C/min in Ar (99.999%) atmosphere with a flow rate of 400 sccm. Subsequently, H_2 (99.999%) and ethylene (99.95%) were introduced in turn at the same temperature with a flow rate of 150 and 200 sccm, respectively, and kept at these conditions for 30 min. Finally the system was cooled to room temperature in an Ar atmosphere. In addition, pure graphene microspheres (thickness range from 3 to 7 nm)[53] and multiwalled CNTs[54] were also used for comparison.

Material Characterization. The as-prepared samples were characterized by X-ray diffraction (XRD, TTR-III), a scanning electron microscope (SEM, Camscan Mx2600FE), a transmission electron microscope (TEM, JEM 2010), an atomic force microscope (AFM, Nanoscope IIIa), and Raman spectroscopy (Jobin-Yvon HR800, 457.9 nm). The Brunauer–Emmett–Teller (BET) surface areas of the samples were measured at 77 K using NOVA 2000 (Quantachrome, USA).

Electrochemical Measurement. Lithium sheets were used as both reference and counter electrodes, and a composite electrode comprising active mass, carbonaceous additive

(acetylene black, 10 wt %) and poly(vinylidene difluoride) (PVDF, 10 wt %) binder was used as the working electrode. A 1 M $LiPF_6$ solution in a 1:1:1 (volume) mixture of ethylene carbonate (EC), ethylmethyl carbonate (EMC), and dimethyl carbonate (DMC) was used as the electrolyte. The density of the electrode materials was 0.628 g/cm^3. The cells were galvanostatically charged and discharged in the voltage range from 0.01 to 3 V *vs* Li/Li^+ at different current densities. The cyclic voltammetry measurement was carried out on a CHI 660C electrochemical workstation at a scan rate of 0.1 mV s^{-1}. The ac impendence spectra were obtained by applying a sine wave with an amplitude of 5.0 mV over the frequency range from 100 kHz to 0.01 Hz.

Acknowledgment. The authors acknowledge financial support from the National Science Foundation of China (Nos. 51077014, 21003028) and Fundamental Research Funds for the Central Universities (HEUCF101006).

REFERENCES AND NOTES

1. Cui, G. L.; Zhi, L. J.; Thomas, A.; Kolb, U.; Lieberwirth, I.; Mullen, K. One-Dimensional Porous Carbon/Platinum Composites for Nanoscale Electrodes. *Angew. Chem., Int. Ed.* **2007,** *46*, 3464–3467.
2. Zhi, L. J.; Hu, Y. S.; El Hamaoui, B.; Wang, X.; Lieberwirth, I.; Kolb, U.; Maier, J.; Mullen, K. Precursor-Controlled Formation of Novel Carbon/Metal and Carbon/Metal Oxide Nanocomposites. *Adv. Mater.* **2008,** *20*, 1727–1731.
3. Rolison, D. R.; Long, R. W.; Lytle, J. C.; Fischer, A. E.; Rhodes, C. P.; McEvoy, T. M.; Bourga, M. E.; Lubers, A. M. Multifunctional 3D Nanoarchitectures for Energy Storage and Conversion. *Chem. Soc. Rev.* **2009,** *38*, 226–252.
4. Yoo, E.; Kim, J.; Hosono, E.; Zhou, H.; Kudo, T.; Honma, I. Large Reversible Li Storage of Graphene Nanosheet Families for Use in Rechargeable Lithium Ion Batteries. *Nano Lett.* **2008,** *8*, 2277–2282.
5. Wang, G.; Shen, X.; Yao, J.; Park, J. Graphene Nanosheets for Enhanced Lithium Storage in Lithium Ion Batteries. *Carbon* **2009,** *47*, 2049–2053.
6. Pan, D. Y.; Wang, S.; Zhao, B.; Wu, M. H.; Zhang, H. J.; Wang, Y.; Jiao, Z. Li Storage Properties of Disordered Graphene Nanosheets. *Chem. Mater.* **2009,** *21*, 3136–3142.
7. Lian, P. C.; Zhu, X. F.; Liang, S. Z.; Li, Z.; Yang, W. S.; Wang, H. H. Large Reversible Capacity of High Quality Graphene Sheets as an Anode Material for Lithium-Ion Batteries. *Electrochim. Acta* **2010,** *55*, 3909–3914.
8. Paek, S. M.; Yoo, E.; Honma, I. Enhanced Cyclic Performance and Lithium Storage Capacity of SnO_2/Graphene Nanoporous Electrodes with Three-Dimensionally Delaminated Flexible Structure. *Nano Lett.* **2009,** *9*, 72–75.
9. Yao, J.; Shen, X.; Wang, B.; Liu, H.; Wang, G. In Situ Chemical Synthesis of SnO_2-Graphene Nanocomposite as Anode Materials for Lithium-Ion Batteries. *Electrochem. Commun.* **2009,** *11*, 1849–1852.
10. Wang, G. X.; Wang, B.; Wang, X. L.; Park, J.; Dou, S. X.; Ahn, H.; Kim, K. Sn/Graphene Nanocomposite with 3D Architecture for Enhanced Reversible Lithium Storage in Lithium Ion Batteries. *J. Mater. Chem.* **2009,** *19*, 8378–8384.
11. Chou, S. L.; Wang, J. Z.; Choucair, M.; Liu, H. K.; Stride, J. A.; Dou, S. X. Enhanced Reversible Lithium Storage in a Nanosize Silicon/Graphene Composite. *Electrochem. Commun.* **2010,** *12*, 303–306.
12. Wang, D. H.; Choi, D. W.; Li, J.; Yang, Z. G.; Nie, Z. M.; Kou, R.; Hu, D. H.; Wang, C. M.; Saraf, L. V.; Zhang, J. G.; *et al*. SelfAssembled TiO_2-Graphene Hybrid Nanostructures for Enhanced Li-Ion Insertion. *ACS Nano* **2009,** *3*, 907–914.
13. Ji, F.; Li, Y. L.; Feng, J. M.; Su, D.; Wen, Y. Y.; Feng, Y.; Hou, F. Electrochemical Performance of Graphene Nanosheets and Ceramic Composites as Anodes for Lithium Batteries. *J. Mater. Chem.* **2009,** *19*, 9063–9067.
14. Yang, S.; Cui, G.; Pang, S.; Cao, Q.; Kolb, U.; Feng, X.; Maier, J.; Müllen, K. Fabrication of Cobalt and Cobalt Oxide/Graphene Composites: Towards High-Performance Anode Materials for Lithium Ion Batteries. *ChemSusChem* **2010,** *3*, 236–239.
15. Guo, P.; Song, H. H.; Chen, X. H. Hollow Graphene Oxide Spheres Self-Assembled by W/O Emulsion. *J. Mater. Chem.* **2010,** *20*, 4867–4874.
16. Su, D.; Schlögl, R. Nanostructured Carbon and Carbon Nanocomposites for Electrochemical Energy Storage Applications. *ChemSusChem* **2010,** *3*, 136–168.
17. Chen, Z.; Qin, Y.; Weng, D.; Xiao, Q.; Peng, Y.; Wang, X.; Li, H.; Wei, F.; Lu, Y. Design and Synthesis of Hierarchical Nanowire Composites for Electrochemical Energy Storage. *Adv. Funct. Mater.* **2009,** *19*, 3420–3426.
18. Novoselov, K. S.; Geim, A. K.; Morozov, S. V.; Jiang, D.; Zhang, Y.; Dubonos, S. V.; Grigorieva, I. V.; Firsov, A. A. Electric Field Effect in Atomically Thin Carbon Films. *Science* **2004,** *306*, 666–669.
19. Novoselov, K. S.; Jiang, D.; Schedin, F.; Booth, T. J.; Khotkevich, V. V.; Morozov, S. V.; Geim, A. K. Two-Dimensional Atomic Crystals. *Proc. Natl. Acad. Sci. U. S. A.* **2005,** *102*, 10451–10453.
20. Novoselov, K. S.; Geim, A. K.; Morozov, S. V.; Jiang, D.; Katsnelson, M. I.; Grigorieva, I. V.; Dubonos, S. V.; Firsov, A. A. Two-Dimensional Gas of Massless Dirac Fermions in Graphene. *Nature* **2005,** *438*, 197–200.
21. Geim, A. K.; Novoselov, K. S. The Rise of Graphene. *Nat. Mater.* **2007,** *6*, 183–191.
22. Geim, A. K. Graphene: Status and Prospects. *Science* **2009,** *324*, 1530–1534.
23. Tung, V. C.; Chen, L. M.; Allen, M. J.; Wassei, J. K.; Nelson, K.; Kaner, R. B.; Yang, Y. Low-Temperature Solution Processing of Graphene-Carbon Nanotube Hybrid Materials for High-Performance Transparent Conductors. *Nano Lett.* **2009,** *9*, 1949–1955.
24. Yu, D.; Dai, L. Self-Assembled Graphene/Carbon Nanotube Hybrid Films for Supercapacitors. *J. Phys. Chem. Lett.* **2009,** *1*, 467–470.
25. Kim, Y. K.; Min, D. H. Durable Large-Area Thin Films of Graphene/Carbon Nanotube Double Layers as a Transparent Electrode. *Langmuir* **2009,** *25*, 11302–11306.
26. Cai, D. Y.; Song, M.; Xu, C. X. Highly Conductive Carbon-Nanotube/Graphite-Oxide Hybrid Films. *Adv. Mater.* **2008,** *20*, 1706–1709.
27. Yu, A. P.; Ramesh, P.; Sun, X. B.; Bekyarova, E.; Itkis, M. E.; Haddon, R. C. Enhanced Thermal Conductivity in a Hybrid Graphite Nanoplatelet−Carbon Nanotube Filler for Epoxy Composites. *Adv. Mater.* **2008,** *20*, 4740–4744.
28. Lee, D. H.; Kim, J. E.; Han, T. H.; Hwang, J. W.; Jeon, S.; Choi, S. Y.; Hong, S. H.; Lee, W. J.; Ruoff, R. S.; Kim, S. O. Versatile Carbon Hybrid Films Composed of Vertical Carbon Nanotubes Grown on Mechanically Compliant Graphene Films. *Adv. Mater.* **2010,** *22*, 1247–1252.
29. Li, C. Y.; Li, Z.; Zhu, H. W.; Wang, K. L.; Wei, J. Q.; Li, X. A.; Sun, P. Z.; Zhang, H.; Wu, D. H. Graphene Nano-"Patches" on a Carbon Nanotube Network for Highly Transparent/Conductive Thin Film Applications. *J. Phys. Chem. C* **2010,** *114*, 14008–14012.
30. Li, B.; Cao, X. H.; Ong, H. G.; Cheah, J. W.; Zhou, X. Z.; Yin, Z. Y.; Li, H.; Wang, J. L.; Boey, F.; Huang, W.; *et al*. All-Carbon Electronic Devices Fabricated by Directly Grown Single-Walled Carbon Nanotubes on Reduced Graphene Oxide Electrodes. *Adv. Mater.* **2010,** *22*, 3058–3061.
31. Liu, C.; Li, F.; Ma, L.-P.; Cheng, H.-M. Advanced Materials for Energy Storage. *Adv. Mater.* **2010,** *22*, E28–E62.
32. Park, M. H.; Kim, K.; Kim, J.; Cho, J. Flexible Dimensional Control of High-Capacity Li-Ion-Battery Anodes: From 0D Hollow to 3D Porous Germanium Nanoparticle Assemblies. *Adv. Mater.* **2010,** *22*, 415–418.
33. Zhao, Z. G.; Ci, L. J.; Cheng, H. M.; Bai, J. B. The Growth of Multi-Walled Carbon Nanotubes with Different Morphologies on Carbon Fibers. *Carbon* **2005,** *43*, 663–665.
34. Wang, S. R.; Zhang, Y.; Abidi, N.; Cabrales, L. Wettability and Surface Free Energy of Graphene Films. *Langmuir* **2009,** *25*, 11078–11081.
35. Chen, X. H.; Deng, F. M.; Lu, X. N.; Wu, G. T.; Wang, M.; Yang, H. S.; Zhang, X. B. Growth of Well-Crystallized Segmented

Graphite Nanofibers by Catalytic Chemical Vapor Deposition. *J. Cryst. Growth* **2001,** *222*, 163–169.
36. Veziri, C. M.; Karanikolos, G. N.; Pilatos, G.; Vermisoglou, E. C.; Giannakopoulos, K.; Stogios, C.; Kanellopoulos, N. K. Growth and Morphology Manipulation of Carbon Nanostructures on Porous Supports. *Carbon* **2009,** *47*, 2161–2173.
37. Yoon, S. H.; Park, C. W.; Yang, H. J.; Korai, Y.; Mochida, I.; Baker, R. T. K.; Rodriguez, N. M. Novel Carbon Nanofibers of High Graphitization as Anodic Materials for Lithium Ion Secondary Batteries. *Carbon* **2004,** *42*, 21–32.
38. Tuinstra, F. Raman Spectrum of Graphite. *J. Chem. Phys.* **1970,** *53*, 1126–1130.
39. Kudin, K. N.; Ozbas, B.; Schniepp, H. C.; Prud'homme, R. K.; Aksay, I. A.; Car, R. Raman Spectra of Graphite Oxide and Functionalized Graphene Sheets. *Nano Lett.* **2008,** *8*, 36–41.
40. Gao, W.; Alemany, L. B.; Ci, L.; Ajayan, P. M. New Insights into the Structure and Reduction of Graphite Oxide. *Nat. Chem.* **2009,** *1*, 403–408.
41. Yang, S.; Feng, X. L.; Zhi, L. J.; Cao, Q.; Maier, J.; Mullen, K. Nanographene-Constructed Hollow Carbon Spheres and Their Favorable Electroactivity with Respect to Lithium Storage. *Adv. Mater.* **2010,** *22*, 838–842.
42. Chen, J.; Wang, J. Z.; Minett, A. I.; Liu, Y.; Lynam, C.; Liu, H.; Wallace, G. G. Carbon Nanotube Network Modified Carbon Fibre Paper for Li-Ion Batteries. *Energy Environ. Sci.* **2009,** *2*, 393–396.
43. Choi, Y. K.; Chung, K. I.; Kim, W. S.; Sung, Y. E. Electrochemical Properties of Passivation Film on Mesophase Pitch-Based Carbon Fiber Electrode. *Microchem. J.* **2001,** *68*, 61–70.
44. Lahiri, I.; Oh, S. W.; Hwang, J. Y.; Cho, S.; Sun, Y. K.; Banerjee, R.; Choi, W. High Capacity and Excellent Stability of Lithium Ion Battery Anode Using Interface-Controlled Binder-Free Multiwall Carbon Nanotubes Grown on Copper. *ACS Nano* **2010,** *4*, 3440–3446.
45. Adelhelm, P.; Hu, Y. S.; Chuenchom, L.; Antonietti, M.; Smarsly, B. M.; Maier, J. Generation of Hierarchical Meso- and Macroporous Carbon from Mesophase Pitch by Spinodal Decomposition using Polymer Templates. *Adv. Mater.* **2007,** *19*, 4012–4017.
46. Habazaki, H.; Kiriu, M.; Konno, H. High Rate Capability of Carbon Nanofilaments with Platelet Structure as Anode Materials for Lithium Ion Batteries. *Electrochem. Commun.* **2006,** *8*, 1275–1279.
47. Zhang, H. L.; Zhang, Y.; Zhang, X. G.; Li, F.; Liu, C.; Tan, J.; Cheng, H. M. Urchin-Like Nano/Micro Hybrid Anode Materials for Lithium Ion Battery. *Carbon* **2006,** *44*, 2778–2784.
48. Jamnik, J.; Maier, J. Treatment of the Impedance of Mixed Conductors—Equivalent Circuit Model and Explicit Approximate Solutions. *J. Electrochem. Soc.* **1999,** *146*, 4183–4188.
49. Yang, S. B.; Song, H. H.; Chen, X. H. Electrochemical Performance of Expanded Mesocarbon Microbeads as Anode Material for Lithium-Ion Batteries. *Electrochem. Commun.* **2006,** *8*, 137–142.
50. Lou, X. W.; Archer, L. A.; Yang, Z. C. Hollow Micro-/Nanostructures: Synthesis and Applications. *Adv. Mater.* **2008,** *20*, 3987–4019.
51. Wang, X.; Zhi, L. J.; Tsao, N.; Tomovic, Z.; Li, J. L.; Mullen, K. Transparent Carbon Films as Electrodes in Organic Solar Cells. *Angew. Chem., Int. Ed.* **2008,** *47*, 2990–2992.
52. Hummers, W. S.; Offeman, R. E. Preparation of Graphitic Oxide. *J. Am. Chem. Soc.* **1958,** *80*, 1339.
53. Wei, T.; Wang, F.; Yan, J.; Cheng, J.; Fan, Z.; Song, H. Microspheres Composed of Multilayer Graphene as Anode Material for Lithium-Ion Batteries. *J. Electroanal. Chem.* **2011,** *653*, 45–49.
54. Wang, Y.; Wei, F.; Luo, G. H.; Yu, H.; Gu, G. S. The Large-Scale Production of Carbon Nanotubes in a Nano-Agglomerate Fluidized-Bed Reactor. *Chem. Phys. Lett.* **2002,** *364*, 568–572.